Clays and Clay Minerals, Vol. 39, No. 3, pp. 254–263, 1991.

HIGH-RESOLUTION TRANSMISSION ELECTRON MICROSCOPY STUDY OF Mn-OXYHYDROXIDE TRANSFORMATIONS AND ACCOMPANYING PHASES IN A LATERITIC PROFILE OF MOANDA, GABON

M. AMOURIC,[1] S. PARC,[2] AND D. NAHON[2]

[1] Centre de Recherche sur les Mécanismes de la Croissance Cristalline
C.N.R.S.–Campus Luminy, case 913, 13288 Marseille Cedex 9, France

[2] Laboratoire de Géosciences de l'Environnement, URA C.N.R.S. 132
Faculté des Sciences de St. Jérôme, case 431, 13397 Marseille Cedex 13, France

Abstract—Unheated natural mixtures of manganite and secondary pyrolusite, from the same lateritic manganiferous sequence, were studied in different orientations by high-resolution transmission electron microscopy (HRTEM), electron diffraction, and energy-dispersive X-ray analysis (EDX) to determine the fine structure of these phases, their possible crystallographic relations, and the genetic processes that led to the formation of the pyrolusite. Typical palisadic texture was observed for both minerals. Characteristic cracks parallel to (010) of the pyrolusite structure and in particular ⟨210⟩ microfissures in manganite were noted as signs of structural accommodation accompanying the transformation phenomenon between these two minerals. A previously unreported manganese oxide of the spinel-type (γ-Mn_2O_3 or Mn_3O_4) was also identified in the original mixture. This oxide gave pure microdomains as intergrowths with pyrolusite adjacent to manganite. This is the first report of a natural occurrence of γ-Mn_2O_3. The manganite-pyrolusite transformation process and an unsuspected γ-Mn_2O_3 (Mn_3O_4)-pyrolusite transition were directly illustrated in detail for the first time. Interfaces between the concerned phases were not sharp or smooth, but exhibited strong strain contrasts and interferential periodicities. Lattice images and microdiffraction patterns proved that both transformations were oriented, suggestive of topotactic relations. In addition, the principal minerals in the matrix (illite, kaolinite, and goethite) were examined for a better understanding of their role in Mn-oxyhydroxides transformations.

Key Words—Energy-dispersive X-ray analysis, Hausmannite, High-resolution transmission electron microscopy, Laterite, Manganese, Manganite, Pyrolusite, Topotactic transformation.

INTRODUCTION

Lateritic weathering of Mn^{2+}-bearing rocks (mainly carbonates and silicates) in tropical and equatorial areas produces complex weathering sequences containing, in particular, various Mn^{3+} and Mn^{4+} oxides and hydroxides. Occurrences and transformations between these minerals are directly related to the weathering process. They are also related to the parent rock composition in that, in general, phases having higher Mn oxidation numbers are more abundant toward the surface. Among the major Mn oxyhydroxides encountered in such sequences, manganite (MnOOH) and pyrolusite (MnO_2) are well crystallized compared with other Mn species. These phases commonly are intimately intermixed. Secondary pyrolusite (its much more common occurrence) is known to develop as pseudomorphic replacements of other Mn oxides, particularly manganite. In fact, pyrolusite (tetragonal) and manganite (monoclinic) have similar rutile-type structures and are based on chains of edge-shared MnO_6 octahedra. Theoretically, the manganite *a* and *c* translations are halved to form the *a* and *c* unit-cell translations of the secondary pyrolusite, and the *b* of manganite contracts from 5.28 to 4.40 Å to form the other *a* translation of pyrolusite (see Rask and Buseck, 1986). No real and direct proof of a possible genetic relation exists, however, and details about possible transformation mechanisms are lacking.

Electron microscopy is, today, an unrivaled method to study the structural properties of minerals, even at the atomic scale. Although several such studies have been made of Mn oxides (see, e.g., Turner and Buseck, 1979, 1981, 1983; Giovanoli, 1985; Perseil and Giovanoli, 1982), only a few have been made of manganite and pyrolusite. Champness was the first (1971), followed by Yamada *et al.* (1986), to demonstrate that microscopic cracks parallel to the pyrolusite (010) planes separated newly made crystallites of pyrolusite. Such cracks were interpreted as a possible final result of manganite lattice accommodation. Also, an intermediate phase (Mn_5O_8) was found by Rask and Buseck (1986) by high-resolution transmission electron microscopy (HRTEM) to be intergrown with pyrolusite that had formed from manganite.

In the present study, unheated natural mixtures of manganite and pyrolusite from the Moanda sequence (Gabon) were examined by HRTEM in an effort to characterize these two phases and to gain a better understanding of the processes responsible for their transformation. Two possible evolution pathways are suggested from these observations. In addition, an

unexpected phase (γ-Mn_2O_3 or Mn_3O_4) was found to play an important role in the formation of the pyrolusite.

GENERAL LITHOLOGY

The lateritic profile was developed on manganiferous sedimentary rocks in the Moanda minefield, Gabon. A global cross section of this profile is shown in Figure 1. Briefly, the Precambrian sedimentary parent rock (level I) is a black calcareous shale, made up of about 56% rhodochrosite, 23% illite, 11% detrital silt-size quartz, 4% pyrite, and 6% organic matter (Parc *et al.*, 1989). In general, the weathering profile (Perseil and Bouladon, 1971; Weber *et al.*, 1979; Nahon *et al.*, 1983; Boeglin, 1981; Beauvais, 1984) consists of bands of manganite + pyrolusite, nearest the bed rock (level II), overlain by cryptomelane, nsutite, a second generation of pyrolusite, and lithophorite (levels III, IV, and V). In this study, we have focused on the so-called "layer-base" (=level I, in Figure 1). Petrographically, the boundary between the rhodochrosite-bearing rock and this manganite-pyrolusite layer is sharp. Manganite crystals replace rhodochrosite, preserving the micronodular texture of the bedrock. The contact between the manganite layer and the pyrolusite layer shows fine indentations (Parc, 1989), which were observed in detail with HRTEM. Above this contact, palisadic crystals of pyrolusite are present, and the matrix is epigenetically invaded by this phase. Generally, in such a profile, the Mn oxidation number increases toward the surface.

EXPERIMENTAL

Manganite-pyrolusite transformation zones were initially recognized and selected under the optical and metallographical microscopes. Parts of selected samples was ion-thinned with a double-gun ion mill, and other parts was ultramicrotomed with a diamond knife after araldite embedding, following the procedures outlined by Amouric and Parron (1985). JEOL JEM 100 C (100 kV) and JEM 2000 FX (200 kV) instruments were used for the HRTEM studies. The latter was equipped with a double-tilt specimen stage and an objective lens having a C_S value of 1.8 mm. Only bright-field images were recorded using reflections passing through a 80-μm objective aperture. Images with optimum defocus (−800 to −1200 Å) were selected from an experimental through-focus series. Semiquantitative microchemical analyses were obtained by energy-dispersive X-ray spectroscopy (EDX) using a Tracor system directly coupled to the JEOL 2000 FX microscope. Standardless analyses were carried out in the TEM mode, using a beam diameter of 50 to 150 Å.

RESULTS

The manganite and pyrolusite occurred at the base of the Moanda sequence. The samples consisted of

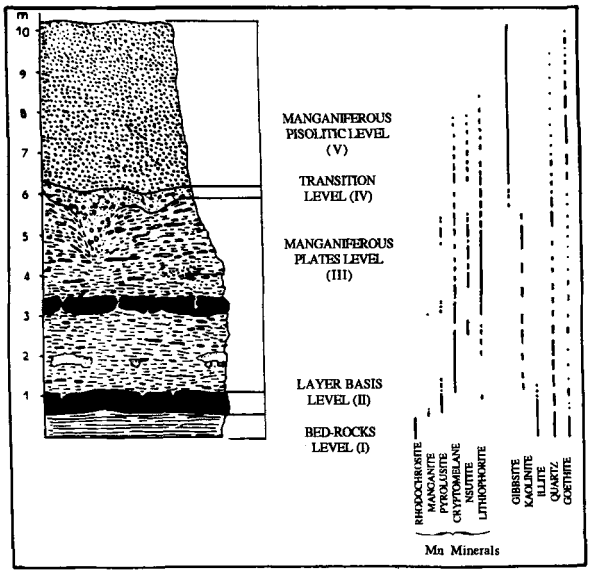

Figure 1. Scheme of lateritic weathering profile developed at Moanda on carbonate parent rock (after Boeglin, 1981) and corresponding mineralogical development.

domains of pure manganite, domains of pure pyrolusite, domains of intergrown manganite-pyrolusite, and of zones of pyrolusite and another phase. The domains were observed in different orientations. A matrix surrounded all the phases.

Manganese oxyhydroxides

Pure manganite. In the present study, observations perpendicular to the *b* axis of manganite were chosen. Figures 2a and 3a are typical low-magnification images of manganite, especially near the manganite-pyrolusite boundary. As viewed along its $\vec{c}$ axis (Figures 2a and 2b), manganite occurs as irregular laths several hundred Ångstroms long and 200–300 Å wide, elongated along the $\vec{b}$ axis. Regular zig-zag fissures and cracks divide these laths into prismatic subgrains, such as those marked A, B, C, . . . , all having a common z-axis direction. In some microtomed specimens, some such fissures may have been slightly opened possibly due to the mechanical effect of the diamond knife; however, the regular and well-marked fissures clearly parallel the ⟨210⟩ manganite direction and so appeared to be significant (Figure 2a). Indeed, such directions may be morphological growth directions for manganite (Valarelli *et al.*, 1969). Moreover these zig-zag fissures were not systematically visible all over the manganite areas. Indeed, farther from the transition front with pyrolusite and viewed in the same $\vec{c}$ direction, manganite generally appeared as undivided blocks.

In another view direction showing its [010]* and [101]* rows (Figure 3b), manganite was noted as laths elongated perpendicularly to the $\vec{b}$ axis (Figure 3a). In

https://doi.org/10.1346/CCMN.1991.0390305 Published online by Cambridge University Press

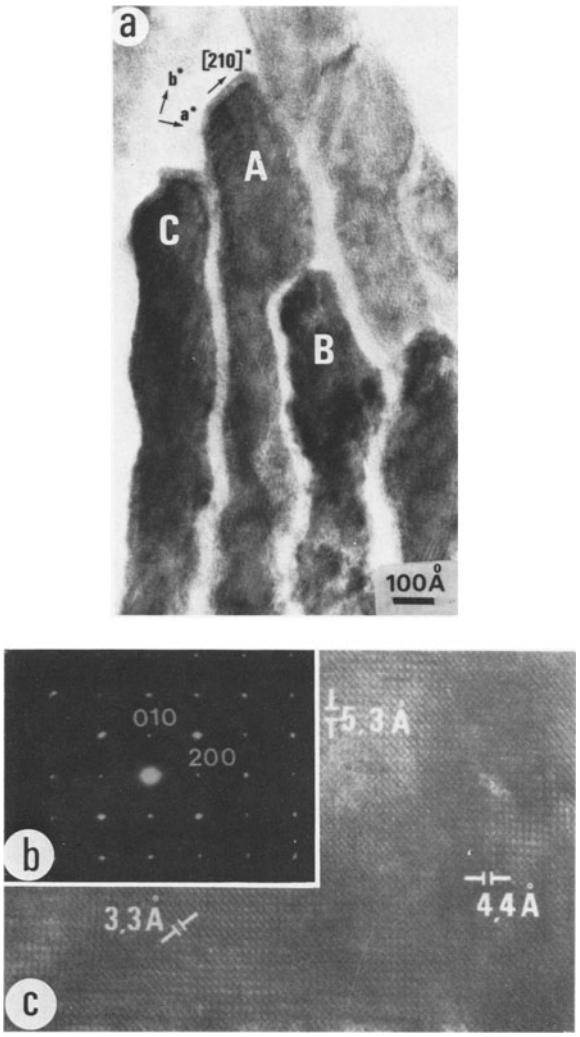

Figure 2. (a) Transmission electron micrograph showing microstructure of manganite, viewed along $\vec{c}^*$, near manganite-pyrolusite boundary. Note quasi-regular and special zig-zag fissures paralleling ⟨210⟩ directions and laths elongated along $\vec{b}$ axis. A, B, C, . . . are composite subgrains of such laths. (b) Electron diffraction pattern of pure manganite viewed along $\vec{c}^*$. (c) Structure image corresponding to (b) and exhibiting characteristic 5.3-Å (010), 4.4-Å (200), and 3.3-Å (210) periodicity of manganite.

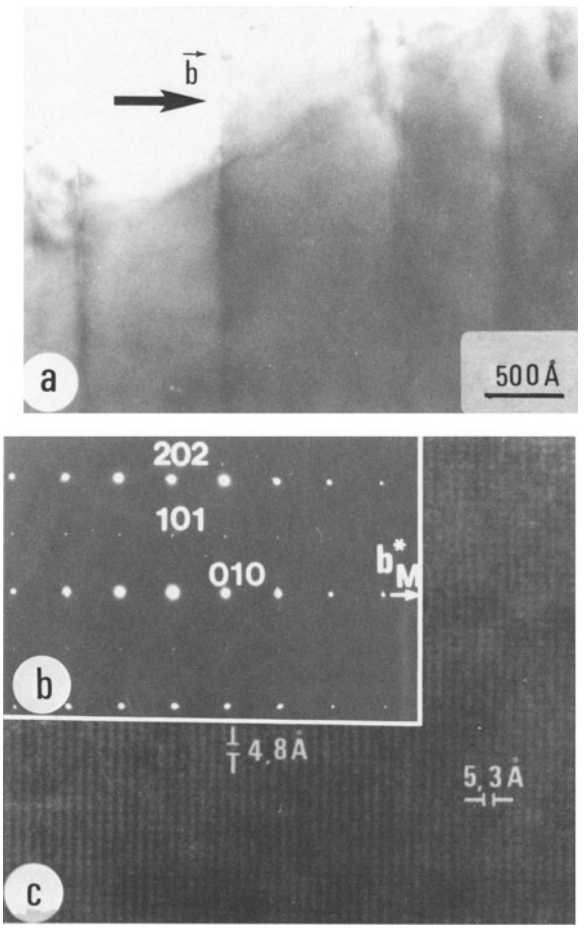

Figure 3. (a) Transmission electron micrograph showing characteristic lath morphology of manganite viewed perpendicular to its $\vec{b}$ axis. (b) Electron diffraction pattern of pure manganite displaying [010]* and [101]* rows. (c) Structure image corresponding to (b) and exhibiting characteristic 4.8-Å (101) and 5.3-Å (010) periodicities of manganite.

this orientation, marks of probable characteristic (010) cleavage were visible, dividing manganite in rectangular parallel laths. Such a particular palisade-like arrangement was also found for pyrolusite if it was viewed in the same direction (Figure 4c).

Figures 2c and 3c are corresponding two-dimensional lattice images of pure manganite and reveal 200,010 and 101,010 lattice spacings, respectively. In the image mode, manganite generally exhibited a uniform appearance with little evidence of crystal strain and defects, except near the transition front (as in Figure 2c) at which a slight mottled contrast was visible.

Manganite in ion-thinned and microtomed samples appeared to be stable under the electron beam over time. Semiquantitative EDX analyses of such a manganite phase ranged from 93 to 98.5 ± 2 atom % for Mn (Table 1), according to the location and the orientation of the zone studied. No other cation was noted in significant amounts.

Pure pyrolusite. Large zones of pyrolusite apparently remained stable in the electron beam under the observation conditions defined above. Figures 4a and 4b, respectively, show an electron-diffraction pattern and a corresponding two-dimensional image of a pure pyrolusite zone viewed in one selected orientation. In the structure image (Figure 4b), a mottled aspect is visible,

https://doi.org/10.1346/CCMN.1991.0390305 Published online by Cambridge University Press

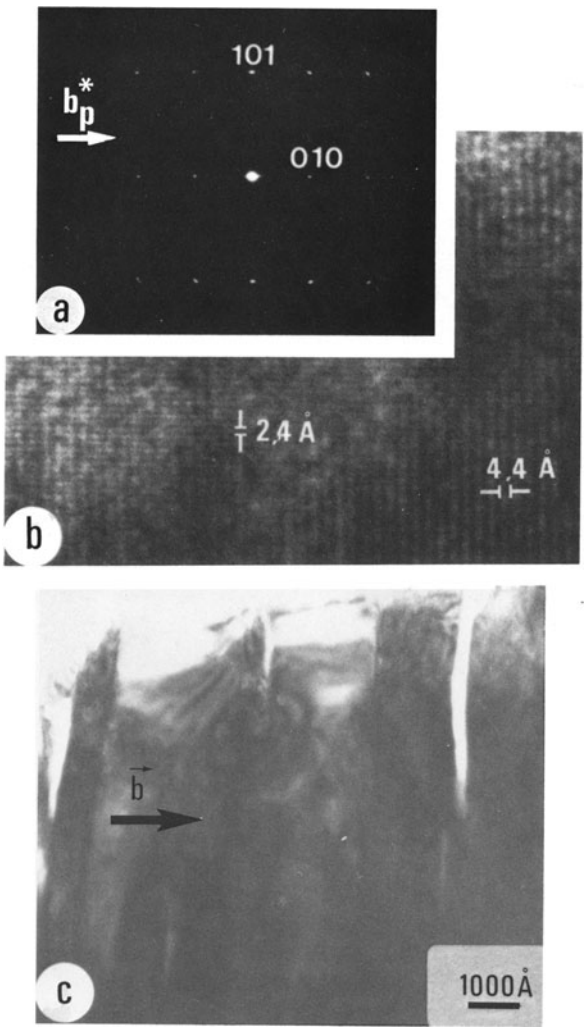

Figure 4. (a) Electron diffraction pattern of pure pyrolusite displaying [010]* and [101]* rows. (b) Structure image of pyrolusite corresponding to (c). Note mottled aspect of pyrolusite. (c) Characteristic lath morphology (in palisade) of pyrolusite and visible cracks, all developed perpendicularly to its $\vec{b}$ axis.

and characteristic 101 and 010 lattice spacings of pyrolusite can be noted. At low magnification (Figure 4c), this pure pyrolusite, oriented as in Figure 4a, consists of pseudo-rectangular lamellar 1500–2000 Å wide, separated by irregular cracks 200–300 Å wide perpendicularly to its $\vec{b}$ axis. Such cracks, parallel to (010), were also found by Champness (1971) and Yamada *et al.* (1986). If a topotactic manganite-pyrolusite transformation is considered, the cracks observed in Figure 4c possibly correspond to the ~15% lattice volume contraction theoretically expected along the $\vec{b}$ axis (Strunz, 1943). Table 1 shows results of a EDX analysis of a pure pyrolusite sample oriented as in Figure 4b. As with manganite, no other cation except Mn was noted in significant amounts.

Table 1. Semiquantitative energy-dispersive X-ray analyses corresponding to the manganite of Figure 3, the pyrolusite of Figure 4b, and accompanying kaolinite.

	Manganite	Pyrolusite	Kaolinite
Mn	98.54	96.93	0.00
Al	0.00	0.00	48.83
Mg	0.00	0.00	0.00
Fe	0.96	1.23	0.00
Si	0.00	1.30	51.17
K	0.00	0.00	0.00
Cr	0.40	0.47	0.00
Ca	0.00	0.06	0.00
Ti	0.00	0.00	0.00
Co	0.00	0.00	0.00

Results are given as atomic percentage of major elements.

Pure γ-Mn_2O_3 or Mn_3O_4. In the same specimens, HRTEM examinations of microtomed and ion-thinned samples revealed the occurrence of a heretofore unreported manganese compound. According to microchemical results (~92% Mn in atom %), this compound was most probably a manganese oxide. It consisted of large, stable, pure laths or microdomains having an apparently regular and well-defined structure. It exhibited homogeneous contrast, but was, in general, intimately intergrown with pyrolusite (Figure 7). Figures 5a and 5b show two selected microdiffraction patterns corresponding to such a phase in two different orientations. By measuring the lattice spacing, a γ-Mn_2O_3 or Mn_3O_4 phase was possibly identified. Its characteristic reflections were 220 and 004 (Figure 5a) and 200 and 020 (Figure 5b) (square lattice). The structures of these two possible tetragonal, pseudo-spinel-type species, as refined by Sinha and Sinha (1957), are crystalographically very similar, making it difficult to distinguish between them.

Oriented intergrowths of manganese oxyhydroxides

Manganite-pyrolusite intergrowth. Very near the manganite-pyrolusite boundary, fine intergrowths of these two phases were noted. The microdiffraction pattern (Figure 6a) shows two-dimensional lattices of pyrolusite and manganite, characterized by strong 101, 010 and 202, 010 reflections, as is also shown in Figures 4c and 3b. Obviously, these two lattices superimpose with their respective rows paralleling each other. The manganite 010 reflection is nearer to the 000 beam than the 010 reflection of pyrolusite. Perpendicularly, the manganite 202 and the pyrolusite 101 reflections perfectly superimpose, and weaker intermediate spots indicate manganite 101 reflections, as in Figure 3b. These two phases are in the exact same orientation, and only their *b* parameters appear to be different. A lattice-fringe image, corresponding to Figure 6a, reveals such an intergrowth (Figure 6b), with thin man-

https://doi.org/10.1346/CCMN.1991.0390305 Published online by Cambridge University Press

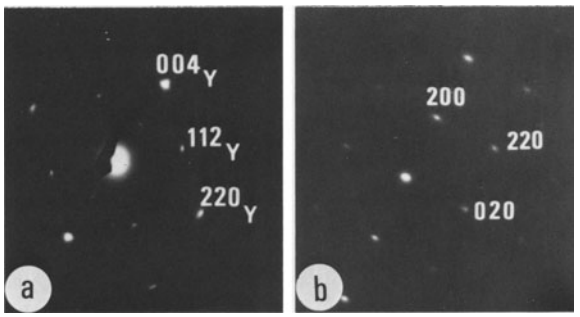

Figure 5. Electron diffraction patterns showing characteristic γ-Mn_2O_3 (or Mn_3O_4) lattice spacings with, respectively, (a) 2.1-Å (220) and 2.36-Å (004) periodicities and (b) 2.9-Å (200)-(020) specific square lattice.

ganite and pyrolusite indentations about 100 to 200 Å wide, irregularly alternating in the $\vec{b}$ direction. In Figure 6c, in which a small part of the transition zone is analyzed in detail, real evidence of cracks or holes is not apparent. Rather, a strong mottled aspect is present in places, probably due to crystal strain incurred during the transition of these two phases. Such strain contrast generally separates laths of different nature and precisely marks the front of evolution between manganite and pyrolusite. Also, as clearly shown by Figures 6b and 6c, the interfaces between these two phases are not at all sharp and smooth. On the contrary, they appear as badly outlined zones 100 Å wide, exhibiting an interferential periodicity as a mixture of adjacent manganite and pyrolusite 010 spacings. On both sides of such interfaces, the respective (010) planes are perfectly parallel to each other.

γ-Mn_2O_3 (or Mn_3O_4)-pyrolusite intergrowth. A γ-Mn_2O_3 (or Mn_3O_4?)-pyrolusite intergrowth was also noted in several places in the same manganite-pyrolusite specimen. This intergrowth, however, was always observed to be perpendicular to the [110] pyrolusite rows. A wide-field micrograph (Figure 7a) shows the intimate structure of zones concerned. It consists of laths of γ-Mn_2O_3 (or Mn_3O_4) elongated along their $\vec{b}$ axis and sandwiched by laths of pyrolusite elongated along their $\vec{c}$ axis (see Figure 7b). Large cracks, 800 to 1600 Å wide, locally separate these laths, but smaller fissures or holes, parallel to the $\vec{c}$ pyrolusite and the $\vec{b}$ direction of γ-Mn_2O_3, are also visible inside the laths where they may be accommodation indicators of a lattice misfit. A corresponding microdiffraction pattern (Figure 7b) indicates two crystal lattices in apparent topotactic conformation. Respectively, the 3.14- and the 2.89-Å reflections probably represent the (110) and (001) planes of pyrolusite and the 2.89- and 4.88-Å reflections, the (020) and (101) planes of γ-Mn_2O_3 (or Mn_3O_4). In the image mode, structural details of such a transition are evident (Figure 7c). Here also, particular strain con-

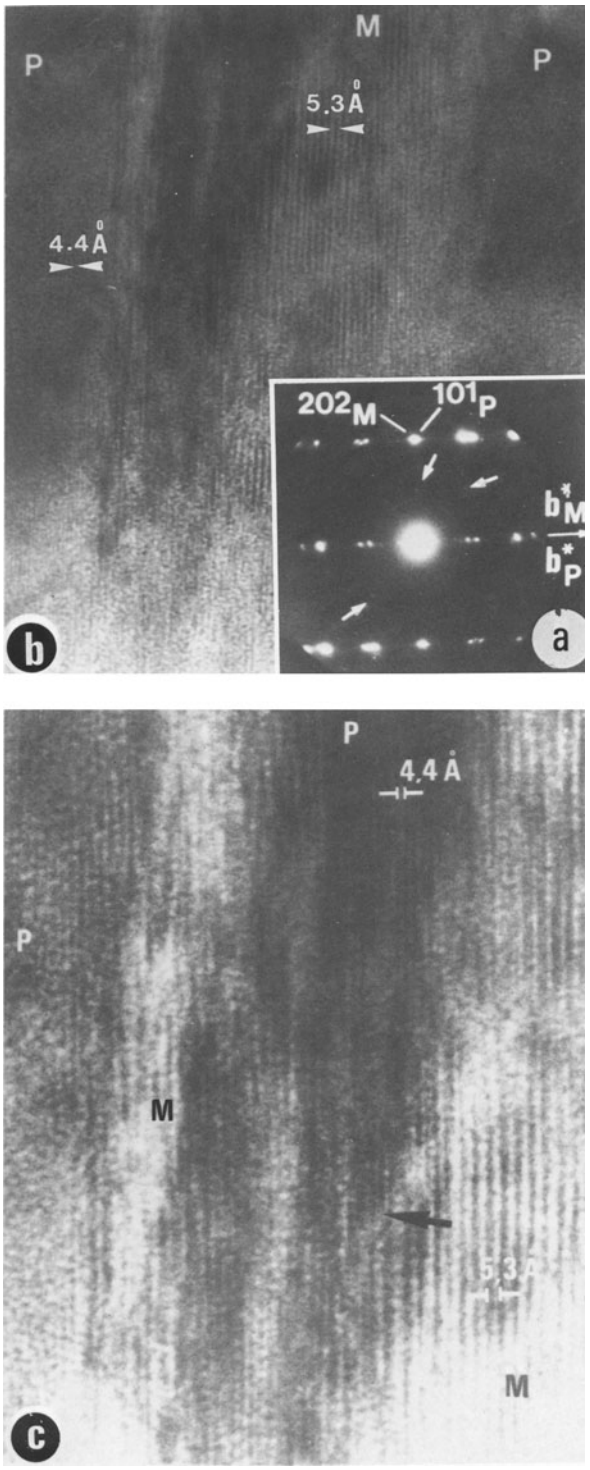

Figure 6. Oriented manganite-pyrolusite intergrowth. (a) Electron diffraction pattern of a pyrolusite (P)-manganite (M) lattices mixture showing respectively (101)*P‖(202)*M reflections and (010)*P‖(010)*M reflections; (b) direct lattice image corresponding to (a); (c) enlarged part of (b) showing details of manganite-pyrolusite transition front (arrow).

https://doi.org/10.1346/CCMN.1991.0390305 Published online by Cambridge University Press

trasts mark the transformation fronts between the two phases and rough interfaces. In fact, such interfaces occur as thin irregular zones, 30 to 60 Å wide, in which lattice fringes are blurred and sometimes vanish. On both sides of the interfaces the (101) planes of γ-Mn_2O_3 (or Mn_3O_4) and the (110) planes of pyrolusite generally parallel each other.

Accompanying phases

Several other coexisting phases, mainly phyllosilicates and iron oxyhydroxides, were also imaged and analyzed with HRTEM.

Phyllosilicates. Among the phyllosilicates observed, illite was the more abundant species and was found mainly with manganite. Generally, illite occurred as large laths several thousand Ångstroms wide and consisted of layered crystallite packets having a well-organized sheet structure (Figure 8a). The phase was identified from its typical 10-Å basal spacing and characteristic low K content. At this level, the manganite development clearly disrupted the illite structure. Figure 8a suggests that illite was pushed back and its structure opened and dissociated into small disoriented particles by the growing manganite. Illite was relatively stable, however, and K was retained in its structure, explaining why cryptomelane species were noted only in samples later in the sequence. HRTEM allowed the detailed stacking sequence of layers of illite along $\vec{c}$ to be seen, and a corresponding polytypic structure could be identified. Figure 8b is a quasi-structure image of a rather thick section of this mineral. A representative two-layer superstructure, having 20 Å periodicity, is present. Such a $2M_1$ form was most commonly observed here. It is the stable polytype of illite (Amouric and Baronnet, 1983; Velde, 1985). Thus, illite is probably an inherited mineral in this geological context.

Locally, kaolinite was identified, mainly in the pyrolusite zone. It consisted of large (>9000 Å wide) pseudo-hexagonal flakes that rapidly damaged under the electron beam. The microchemical data (Table 1) confirm this identification. Given its large size, such a kaolinite was probably detrital.

Iron oxyhydroxides. Most of the iron oxyhydroxides in the specimens were identified as goethite. This goethite mainly occurred as nodules and as pseudomorphic or free laths and spindles. The nodule texture is shown at low magnification in Figure 9. The nodules are generally more or less rounded but, in detail, a primary polygonal habit is still visible, probably inherited from a pre-existing structure. As seen in Figure 9, the core consists of non-equant and randomly oriented particles. A noticeable interparticle porosity can also be recognized. Such nodules are generally coated with a very dark noncrystalline film strongly resembling a gel, as was observed by Amouric *et al.* (1986). The particles are mainly elongated laths, possibly cor-

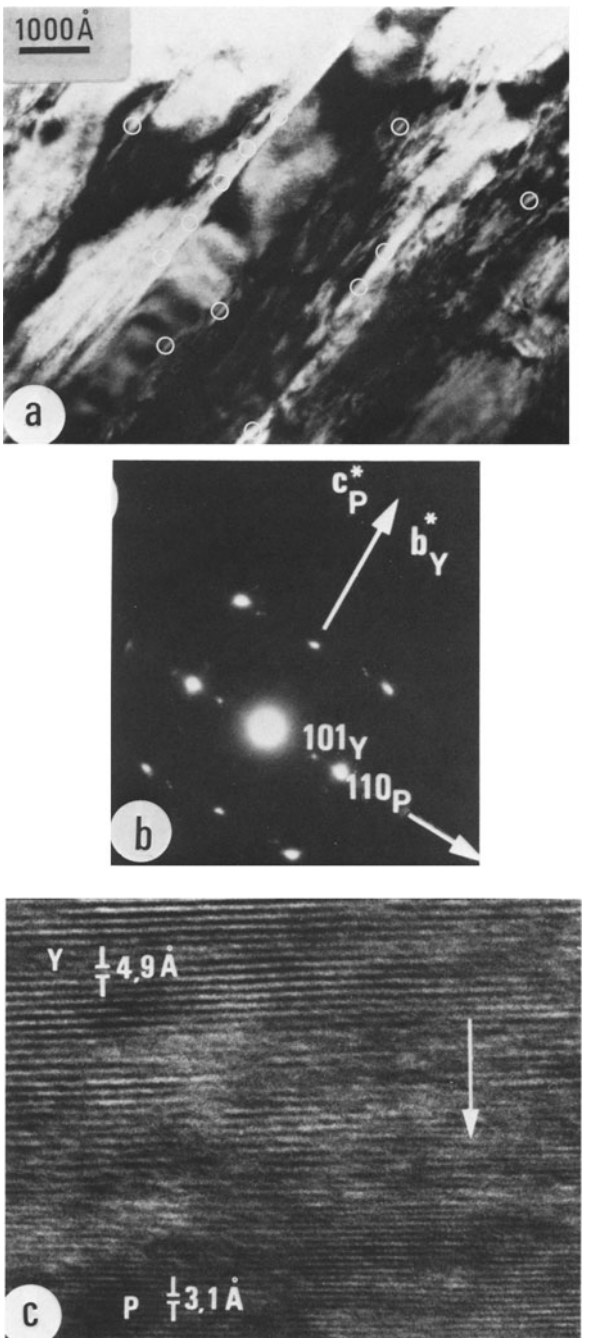

Figure 7. Oriented γ-Mn_2O_3 (or Mn_3O_4)(Y)-pyrolusite (P) intergrowth. (a) Wide field transmission electron image of transition zone of these two phases showing mixed laths. [Note large and smaller cracks (circled) parallel to these laths.] (b) Corresponding electron diffraction pattern displaying (020)*Y‖(001)*P and (101)*Y‖(110)*P reflections; (c) enlarged part of (a) showing out details of γ-Mn_2O_3 (or Mn_3O_4)-pyrolusite transition front.

https://doi.org/10.1346/CCMN.1991.0390305 Published online by Cambridge University Press

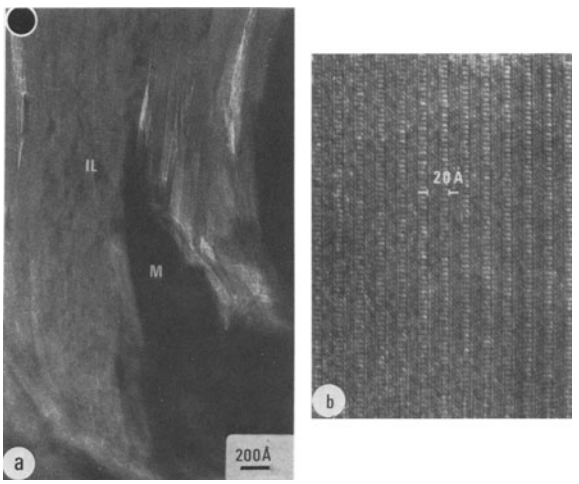

Figure 8. (a) Transmission electron micrograph showing packets of well-organized sheet structure having a characteristic 10-Å basal spacing (=illite) in the matrix. Note the particular manganite(M)-illite(Il) contact. (b) Corresponding structural image of illite exhibiting a $2M_1$ polytypic form.

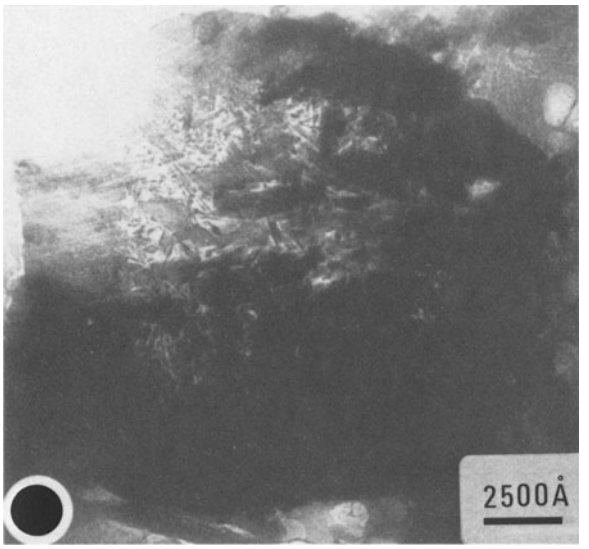

Figure 9. Transmission electron microscope image of apparently rounded iron oxyhydroxide nodule. Note non-equant laths and spindles randomly oriented in the core with significant inter-particle porosity and the gel-like aspect of the periphery.

responding to a fibrous texture of goethite, as reported by Dixon *et al.* (1983) and Amouric *et al.* (1986). Perfect rhombic sections are also present as typical cross sections of goethite laths. The corresponding microchemical data (Figure 11) support these structural analyses. The random orientation and the clear euhedral habit of goethite laths or spindles suggest, as does the large porosity observed, goethite crystals protruding into voids after probable dissolution of most of the previous nodules of pyrite. This goethite probably replaced pyrite which occurs as small grains in the parent rock.

Figure 10 illustrates another occurrence of goethite as apparent flakes having a pseudo-hexagonal habit, near the rhodochrosite zone. In fact, such pseudo-hexagonal morphologies exhibit a composite aspect. As shown in Figure 10, these flakes are clearly divided into subgrains, such as those labeled A, B, C, ... A ⟨110⟩ morphology of typical rhombic sections of goethite is distinguishable. Corresponding microchemical data, similar to those in Figure 11, confirm the presence of goethite. Lastly, these apparent hexagonal flakes locally display regularly spaced linear contrasts (Figure 10). Such lattice figures have periodic spacings of 10.2 and 4.6 Å and are interpreted, respectively, as the (010) and (100) planes of goethite. From these observations, this type of goethite appears to be the product of pseudomorphic transformation that developed perpendicular to the basal planes of preexisting kaolinite.

DISCUSSION AND CONCLUSIONS

Until now, only one HRTEM examination of pure manganite has been published (Rask and Buseck, 1986; Figure 4a). Their observations, however, were made along the *b* axis of manganite, which is crystallographically the less interesting direction in terms of the possible solid transformation of this mineral into pyrolusite. Also, only few HRTEM studies of pyrolusite have been reported (e.g., Rask and Buseck, 1986; Yamada *et al.*, 1986). Yamada *et al.* (1986) reported that pyrolusite rapidly transformed into another oxide under the incident beam, due to the very high voltage they used (1 MV). In the present study, pure manganite and secondary pyrolusite from the same lateritic sequence were characterized and their relations were observed in detail in different crystallographic orientations with HRTEM. These two phases were perfectly stable under the electron beam in the conventional conditions used here and defined above.

Cracks parallel to (010) were observed in pyrolusite (Figure 4c), which may correspond to extended micropores previously noted by some authors who viewed this mineral in the appropriate orientation. They are interpreted here as a mark of a final stage in the manganite-to-pyrolusite transformation. Presumably, the cracks that developed as a result of such a transformation provided channels for the escape of H_2O from manganite and/or facilitated migration of oxygen into the crystals (Rask and Buseck, 1986).

More unusual are the narrow zig-zag cracks developed in manganite parallel to its {210} morphology and seen only near the transition front (Figure 2a). Such an intimate texture of manganite is significant because (210) planes are not cleavage planes of this mineral. Also, based on the P.B.C. (periodic bond chain) theory

https://doi.org/10.1346/CCMN.1991.0390305 Published online by Cambridge University Press

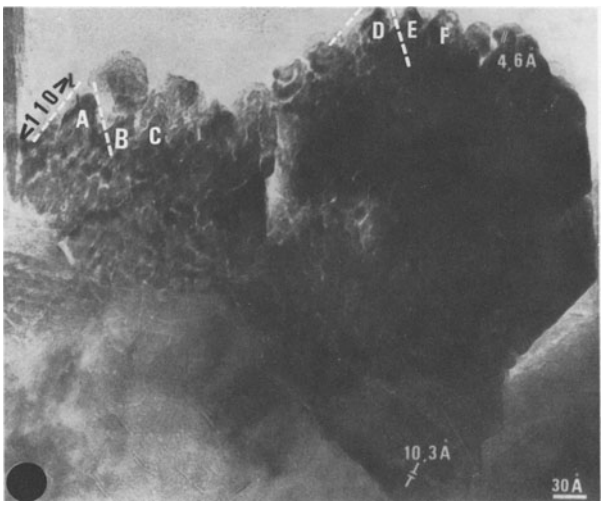

Figure 10. Transmission electron microscope image of apparent pseudohexagonal iron oxyhydroxide. Note composite aspect of such pseudohexagonal morphologies with characteristic rhombic subgrains (A, B, C, . . .) as cross sections of goethite fibers. (A ⟨110⟩ morphology of goethite spindles is visible). Typical 10.2-Å (010) and 4.6-Å (100) goethite lattice spacings are also recognizable.

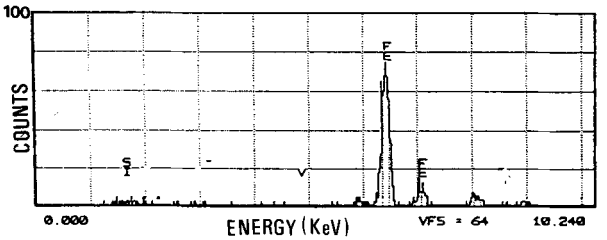

Figure 11. Qualitative energy-dispersive X-ray spectrum corresponding to the goethite laths in the core of iron nodules (Figure 9).

of Hartman and Perdock (1955), Valarelli et al. (1969) demonstrated that (210) was an "F" face type, and thus a possible stable face for the manganite morphology. Lacroix (1962) reported from macroscopic observations that {210} morphology was common in partially dehydrated natural manganite. Lastly, from structural data, H atoms of manganite are apparently localized along its (210, $\bar{2}10$) planes. Such data strongly suggest that the ⟨210⟩ fissures observed in manganite are not fractures but probably resulted from the structural accommodation of this mineral before it completely transformed into pyrolusite. That means that manganite material probably began to contract in the process of phase transformation by partial loss of H. This process may be regarded as a first transition stage.

Pure zones of an unsuspected manganese oxide, exhibiting a tetragonal lattice, adjacent to the manganite and pyrolusite, have been found. This new phase was observed in both ion-thinned and microtomed specimens. This phase probably did not grow or develop in the electron beam under the conditions we used in the present study. Also, most of this compound was detected intergrown with pyrolusite (Figures 7a, 7b, and 7c) and, hence, was not an artifact of HRTEM observation. It was not detected by XRD, probably because of its relative scarcity compared to other manganese oxides present. Whether this phase is γ-$Mn^{3+}O_2$ or $Mn^{3+}Mn^{2+}O_4$ (=hausmannite) is still questionable due to the structural similarities of these two species. This ambiguity is well known in the literature. Only the capability to determine the manganese oxidation states by using electron energy-loss spectroscopy, as was done by Rask *et al.* (1987), could help in this way.

In the literature, γ-Mn_2O_3 is known only as an experimental phase. It has been reported by some authors as obtained under various conditions which often give quite different results (see, for example, Maiti *et al.*, 1983 and Villacieros *et al.*, 1984). Conclusions from such experiments are not clear. Recently, Hernan *et al.* (1986) studied the thermal decomposition products of manganite in vacuo. They found γ-Mn_2O_3 as the initial transformation phase resulting from manganite dehydration at about 250°C. At the same temperature (~250°C), but in dry air, Dent-Glasser and Smith (1968) obtained directly pyrolusite starting from manganite. Therefore, the formation of γ-Mn_2O_3 is probably very sensitive to the environmental medium conditions. By another means, Yamada *et al.* (1986) possibly obtained γ-Mn_2O_3 by the transformation of pyrolusite in the beam of a 1 MV electron microscope; however these authors were not sure of their identification and hesitated, as we do, to distinguish between this phase and hausmannite. Under observation conditions similar to those employed in the present study, Rask and Buseck (1986) and Champness (1971) did not detect γ-Mn_2O_3 accompanying manganite or pyrolusite during HRTEM or TEM studies.

Mn_3O_4 (hausmannite) is known both as an experimental and natural phase. For example, Hernan *et al.* (1986) observed it later in the decomposition sequence of manganite, after γ-Mn_2O_3, by increasing the temperature (>300°C) in vacuo. Starting separately from manganite and pyrolusite, Dent-Glasser and Smith (1968) also obtained Mn_3O_4 directly by hydrothermal treatment (respectively, 400°C, P_{H_2O} = 310 bar and 400°C, P_{H_2O} = 300 bar plus manganese metal). Although it is relatively scarce and not easily detected, hausmannite has also been reported in petrographical analyses at the base of lateritic alteration profiles, having formed from manganese carbonate parent rock (rhodochrosite) (Parc, 1989). From thermodynamical considerations, the stability field of hausmannite, as is that of manganite, is limited in weathering environments (Parc *et al.*, 1989). This probably explains their relative scarcity and the fact that both species are gen-

https://doi.org/10.1346/CCMN.1991.0390305 Published online by Cambridge University Press

erally not abundant (Nahon *et al.*, 1983) in supergene alteration profiles. Thermodynamic data and petrographical descriptions of different Mn-carbonate weathering sequences indicate that hausmannite forms before manganite. The two phases, therefore, appear to be transition phases between the carbonate of reducing environments (rhodochrosite) and the dioxides of oxidizing environments (here, mainly pyrolusite).

The reported experimental conditions are too far from the probable low-temperature occurrence of γ-Mn_2O_3 (Mn_3O_4?) at Moanda. Hence, such considerations do not permit a distinction to be made between the two possible phases. Logically, hausmannite is more probable than γ-Mn_2O_3, according to its reported natural occurrence and to its place generally at the base of Mn-oxyhydroxides sequences. With respect to its intermediate oxidation state, however, hausmannite should be observed in intergrowths also with manganite, which is not evident from the present HRTEM investigations. Therefore, under these conditions, at the basis of Moanda sequence, hausmannite is probably the first alteration product of rhodochrosite, along with manganite, but in less-oxidized microdomains. Subsequently, both these phases transform directly into pyrolusite, in more oxidizing conditions.

For the first time, the manganite-pyrolusite transformation has been directly visualized. In addition, an unexpected and heretofore unknown natural and direct γ-Mn_2O_3 (or Mn_3O_4)-to-pyrolusite transformations has been revealed and illustrated by means of HRTEM. Lattice images showing intergrowths of such phases (Figures 6b, 6c, and 7c), and the corresponding microdiffraction patterns (Figures 6a and 7b) indicate that both transformations are oriented and strongly suggest topotactic conformations according to the Bonev terminology (1972). These transformations imply misfits between respective crystal lattices. Accommodations for these misfits result in various cracks, fissures, small holes, and strain contrast visible in pyrolusite (Figure 4c) and at the manganite-pyrolusite and γ-Mn_2O_3 (Mn_3O_4)-pyrolusite interfaces (Figures 6c and 7a). Manganite and pyrolusite have very related structures, both of rutile type. As for manganite-to-pyrolusite transformation, most authors have suggested that it takes place by the migration of protons out of the manganite structure together with a slight movement of the Mn–O octahedra (Strunz, 1943; Dent-Glasser and Smith, 1968). The mechanism of such a reaction seems therefore to be relatively simple and possible.

On the contrary, the spinel-type structure of γ-Mn_2O_3 (or Mn_3O_4) is quite different from the rutile-type structure of pyrolusite. So, a priori, a γ-MnO_3-to-pyrolusite transformation (and the reverse) seems more complex and implies a greater structural rearrangement such that the corresponding reaction probably needs from the system more energy than does the manganite-to-pyrolusite transformation. (This is an additional reason to assume that the spinel-type structure detected here is not an intermediate phase between manganite and pyrolusite. Indeed, the complete rutile-to-spinel-to-rutile structural reorganization implied in this last reaction would need twice as much energy as the simple γ-Mn_2O_3-to-pyrolusite reaction). Nevertheless, the HRTEM observations (images and microdiffraction patterns) of a natural unheated manganite-pyrolusite mixture reported here suggest that a spinel-type structure (γ-Mn_2O_3 or Mn_3O_4) is in oriented intergrowth with pyrolusite, and that this reaction occurs at low temperature. Thus, the supposed complexity of a rutile-to-spinel-like structure transformation (or the reverse) is not, apparently, a sufficient criterion to prevent such a reaction from occurring in natural specimens, at low temperature.

Lastly, on the assumption that the spinel-type phase observed is hausmannite, we do not completely agree with Dent-Glasser and Smith (1968) concerning the particular crystallographic relations in a possible hausmannite-to-pyrolusite transformation (or the reverse). Indeed, using single crystal X-ray diffraction methods, these authors found hausmannite after hydrothermal treatment of starting pyrolusite to be oriented as follows: $(001)_{Py} \| (010)_{Haus}$ and $(010)_{Py} \| (101)_{Haus}$. For the probable reverse transition, lattice images (Figures 7b and 7c) clearly demonstrated the following orientation relationships: $(010)_{Haus} \| (001)_{Py}$ and $(101)_{Haus} \| (110)_{Py}$. Thus, our results correspond only partly with those of Dent-Glasser and Smith (1968).

REFERENCES

Amouric, M. and Baronnet, A. (1983) Effect of early nucleation conditions on synthetic muscovite polytypism as seen by HRTEM: *Phys. Chem. Miner.* **9,** 146–159.

Amouric, M. and Parron, C. (1985) Structure and growth mechanism of glauconite as seen by HRTEM: *Clays & Clay Minerals* **33,** 473–482.

Amouric, M., Baronnet, A., Nahon, D., and Didier, P. (1986) Electron microscopic investigations of iron oxyhydroxides and accompanying phases in lateritic iron-crust pisolites: *Clays & Clay Minerals* **34,** 45–52.

Beauvais, A. (1984) Concentrations manganesifères latéritiques; étude pétrologique de deux gites sur roches sédimentaires précambriennes: Gisement de Moanda (Gabon) et d'Azul (Brésil): Ph.D. thesis, University of Poitiers, Poitiers, France, 156 pp.

Boeglin, J. L. (1981) Minérologie et Géochimie des gisements de manganèse de Conseilheiro Lafaiete au Brésil et de Moanda au Gabon: Ph.D. thesis, University of Toulouse, Toulouse, France, 155 pp.

Bonev, I. (1972) On the terminology of the phenomena of mutual crystal orientation: *Acta Crystallogr.* **A 28,** 508–512.

Champness, P. E. (1971) The transformation manganite→pyrolusite: *Mineral. Mag.* **38,** 245–248.

Dent-Glasser, L. S. and Smith, I. B. (1968) Oriented transformations in the system MnO-O-H_2O: *Mineral. Mag.* **36,** 976–987.

Dixon, J. B., Golden, D. C., Calhoun, F. G., and Buseck, P. R. (1983) Synthetic aluminous goethite investigated by HRTEM: in *Proc. 41st Annual Meeting Electron Micros-*

copy Soc. Amer., Phoenix, Arizona, 1982, J. W. Bailey, ed., San Francisco Press, San Francisco, 192–193.

Giovanoli, R. (1985) Layer structures and tunnel structures in manganates: *Chem. Erde.* **44,** 227–244.

Hartman, P. and Perdok, W. G. (1955) Relations between structure and morphology of crystals: *Acta Crystallogr.* **8,** 49–52.

Hernan, L., Morales, J., and Tirado, J. L. (1986) Relationships between composition and surface properties of the dehydration products of synthetic manganite: *Surface and Coatings Technology* **27,** 343–350.

Lacroix, A. (1962) *Minéralogie de la France et de ses Anciens Territoires d'Outre-Mer:* Tome **3,** Librairie Scientifique et Technique, A. Blanchard, ed., Paris, pp. 653–670.

Maiti, S., Malessa, O., and Baerns, J. P. (1983) Iron/manganese oxide catalyst for Fischer-Tropsch synthesis. Part I: Structural and textural changes by calcination, reduction and synthesis: *Applied Catalysis* **5,** 151–170.

Nahon, D., Beauvais, A., Boeglin, J. L., Ducloux, J., and Nziengui-Mapangou, P. (1983) Manganite formation in the first stage of the lateritic manganese ores in Africa: *Chem. Geol.* **40,** 25–42.

Parc, S. (1989) Contribution à l'étude cristallochimique et thermodynamique des oxy-hydroxydes de manganèse dans l'altération latéritique: Ph.D. thesis, University of Marseille, Marseille, France, 128 pp.

Parc, S., Nahon, D., Tardy, Y., and Vieillard, P. (1989) Estimated solubility products and fields of stability for cryptomelane, nsutite, birnessite and lithiophorite based on natural lateritic weathering sequences: *Amer. Mineral.* **74,** 466–475.

Perseil, E. A. and Bouladon, J. (1971) Microstructures des oxydes de manganèse à la base du gisement de Moanda et leur signification génétique: *C.R. Acad. Sci., Paris* **273,** 278–279.

Perseil E. A. and Giovanoli, R. (1982) Etude comparative de la Todorokite d'Ambollas des manganates à 10 Å des nodules polymétalliques des océans et des produits de synthèse: *C.R. Acad. Sci., Paris* **294,** 199–202.

Rask, J. H. and Buseck, P. R. (1986) Topotactic relations among pyrolusite, manganite and Mn_5O_8: A HRTEM investigation: *Amer. Mineral.* **71,** 805–814.

Rask, J. H., Miner, B. A., and Buseck, P. R. (1987) Determination of manganese oxidation states in solids by EELS: *Ultramicroscopy* **21,** 321–326.

Sinha, K. P. and Sinha, A. P. B. (1957) Vacancy distribution and bonding in some oxides of spinel structure: *J. Phys. Chem.* **61,** 758–761.

Strunz, H. (1943) Beitrag zum Pyrolusitproblem: *Naturwissenschaften* **31,** 89–91.

Turner, S. and Buseck, P. R. (1979) Manganese oxide tunnel structures and their intergrowths: *Science* **203,** 456–458.

Turner, S. and Buseck, P. R. (1981) Todorokites: A new family of naturally occurring manganese oxides: *Science* **212,** 1024–1027.

Turner, S. and Buseck, P. R. (1983) Defects in nsutite (γ-MnO_2) and dry-cell battery efficiency: *Nature* **304,** 143–146.

Valarelli, J. V., Hypolito, R., Simon, B., Pierrot, M., and Kern, R. (1969) Relaçao entre a estrutura e a morfologia de manganita, à luz da theoria de P.B.C.: *Ciencia Cultura* **21,** 209.

Velde, B. (1985) *Clays Minerals:* Elsevier, Amsterdam, Netherlands, 427 pp.

Villacieros, R. G., Hernan, L., Morales, J., and Tirado, J. L. (1984) Comments on the paper "Iron/manganese oxide catalyst for Fischer-Tropsch synthesis. Part I: Structural and textural changes by calcination, reduction and synthesis" by Maiti et al., *Appl. Catalysis* **5,** 151–170: *Appl. Catalysis* **9,** 133–135.

Weber, F., Leclerc, J., and Millot, G. (1979) Epigénies manganésifères successives dans le gisement de Moanda: *Sci. Geol. Bull.* **32,** 147–164.

Yamada, N., Ohmasa, M., and Horiuchi, S. (1986) Textures in natural pyrolusites, β-MnO_2, examined by 1 MV HRTEM: *Acta Crystallogr.* **B 42,** 58–61.

(Received 14 June 1990; accepted 18 November 1990; MS. 2021)